# Dynamics of a fermion in the Kondo-lattice model for strongly correlated systems

A. Ramšak and P. Prelovšek
*J.Stefan Institute, University of Ljubljana, YU-61111 Ljubljana, Yugoslavia*
(Received 4 May 1990)

The motion of a single fermion coupled to the planar antiferromagnetic spin background is examined within the Kondo-lattice model, including the local spin-fermion coupling and the spin-dependent hopping. The perturbation theory using lowest-order magnon processes and the self-consistent calculation of the quasiparticle spectra, yields several features obtained by an analogous treatment of the $t$-$J$ model by Kane *et al.* Qualitative differences are, however, found in low excited states with the self-energy showing a nonanalytical behavior $\Sigma''(\omega > 0) \propto \omega^{\alpha}$, $\alpha \leq 1$, due to the local Kondo-like coupling. Within the perturbation theory we get $\alpha$=1, while the self-consistent treatment yields $\alpha = \frac{1}{2}$. The modified self-consistent equations lead also to better results for the quasiparticle mass.

## I. INTRODUCTION

In order to understand the character of quasiparticles (QP's) in strongly correlated systems, with superconducting copper oxides as a prominent representative, a number of authors have so far considered the problem of a single charge carrier introduced by doping the planar antiferromagnetic (AFM) insulator. The results obtained by the retraceable-path method,[1,2] by self-consistent treatment of spectral functions[3-5] and by the exact diagonalization of small systems[6-8] yield a reasonable description of the overall behavior of the QP's strongly coupled to the AFM spin system. Yet there are several aspects that need further clarification. One of the most important qualitative questions is the correct description of the low-frequency excited spectra, connected with the existence of the QP peak and its dispersion.

Several models for the AFM insulator doped with a low concentration of mobile holes have been studied. It has been shown[9,10] that in the relevant parameter regime the spin-hole (fermion) models[10-12] as well as the effective single-band $t$-$J$ model[13] represent the qualitative features of more complete two-band Hubbard model for the $CuO_2$ layers in superconducting oxides well. Most theoretical work has been done so far on the prototype $t$-$J$ model.[13] A simple and physically transparent analytical description of a single QP has been introduced by the self-consistent approach.[3-5] Using the representation of the $t$-$J$ model in terms of the slave fermions and Schwinger bosons, the problem of the hole dynamics is effectively mapped on a more ordinary model of a fermion linearly coupled with spin waves. The self-consistent treatment of the latter system yields sensible results for the QP dispersion, for the general structure of excited states, etc. The main conceptual disadvantage of this approach seems to be in the form of the effective coupling between the fermion and the AFM magnons, which appears only through the fermion hopping. On the other hand, the strong on-site interaction due to local constraint does not appear in this effective model, since the constraint is treated in the mean-field manner.

In order to test the validity of the above-mentioned results, we investigate the alternative model, which directly incorporates the local interaction. We start with the generalized Kondo-lattice (spin-hole) model[10-12] for a fermion coupled to the AFM spin system,

$$H = -t_0 \sum_{(ij)s} c^{\dagger}_{is} c_{js} + J \sum_{<ij>} [S^z_i S^z_j + \tfrac{1}{2}\kappa(S^+_i S^-_j + S^-_i S^+_j)] + V \sum_i \mathbf{s}_i \cdot \mathbf{S}_i + t_1 \sum_{(ij)ss'} \tfrac{1}{2}\boldsymbol{\sigma}_{ss'} \cdot \mathbf{S}_i (c^{\dagger}_{is} c_{js'} + c^{\dagger}_{js} c_{is'}) \, . \tag{1.1}$$

The free fermion hopping $t_0$ part and the Heisenberg model for localized spins $\mathbf{S}_i$ are coupled via two types of terms, i.e., the local Kondo-type ($V$) term and the hopping-induced ($t_1$) coupling. The Kondo-lattice model, has been studied in connection with single QP properties by several authors.[11,8,14] It has been also shown that, taking into account the ($t_1$) term, the model represents a very good description of low-lying QP states in the two-band Hubbard model.[10] For realistic large values of $V$ it maps onto the $t$-$J$ model due to the formation of local singlets, formed from a fermion and the local spin. The model, Eq. (1.1), can be thus regarded as equivalent to the $t$-$J$ model (for larger $V$). It has, however, a technical advantage by allowing a more straightforward derivation of the fermion-magnon interaction and the possibility of the perturbative treatment of the latter.

Since our main aim is the study of low-frequency dynamics, we shall, in the following, apply to Eq. (1.1) the

 

expansion of spin operators $\mathbf{S}_i$ into spin waves, based on the existence of the AFM long-range order at $T=0$. The existence of the QP and the low excited states can then be studied by the usual perturbation approach, as followed recently for the Kondo-lattice model also by Furukawa and Imada.[14] The authors pointed out on the logarithmic singularities in the fermion self-energy $\Sigma(\omega)$, having origin in nonlinear magnon-fermion coupling terms. We shall argue that these terms sum up yielding a regular QP band. On the other hand we would rather find a singular low-frequency behavior of $\Sigma(\omega)$, which is governed by the local Kondo-like ($V$ term) coupling.

In Sec. II we derive the fermion-magnon (boson) Hamiltonian corresponding to the model (1.1). Section III is devoted to the perturbative calculation of the self-energy $\Sigma(\omega)$, both for the localized and the mobile fermion. The emphasis is on the low-$\omega$ regime. In Sec. IV we introduce self-consistent equations for $\Sigma(\omega)$. They are solved analytically for the limiting cases of the Ising-type interaction $\kappa \to 0$ in Eq. (1.1) with a weak magnon dispersion. In the special case $V=0$ the set of equations appears to be the same as obtained by Kane *et al.*[4] Our method for finite $V$ can be thus interpreted as an improvement over their method. Results will be shown to differ qualitatively in the small $\omega$ regime, but also quantitatively with respect to QP coherent masses, etc. More general examples are examined by the numerical solution of equations. The extension to finite temperatures $T$ is briefly mentioned in Sec. V. In the Appendix we discuss the influence of nonlinear magnon terms via the variational approach.

## II. FERMION-MAGNON HAMILTONIANS

Assuming the Néel AFM with the staggered wave vector $\mathbf{q}_0 = (\pi, \pi)$ as the reference spin state, we introduce the usual truncated Holstein-Primakoff representation of spins in terms of bosonic operators $a_i, a_i^\dagger$,

$$S_i^{\pm} \cong \tfrac{1}{2}(1 \pm e^{i\mathbf{q}_0\cdot\mathbf{R}_i})a_i + \tfrac{1}{2}(1 \mp e^{i\mathbf{q}_0\cdot\mathbf{R}_i})a_i^\dagger \ , \tag{2.1}$$

$$S_i^z \cong e^{i\mathbf{q}_0\cdot\mathbf{R}_i}(\tfrac{1}{2} - a_i^\dagger a_i) \ . \tag{2.2}$$

Performing the Bogoliubov transformation of operators $a_i$ we get

$$\begin{pmatrix} \alpha_{-\mathbf{q}} \\ \alpha_{\mathbf{q}}^\dagger \end{pmatrix} = \begin{pmatrix} u_{\mathbf{q}} & -v_{\mathbf{q}} \\ -v_{\mathbf{q}} & u_{\mathbf{q}} \end{pmatrix} \begin{pmatrix} b_{-\mathbf{q}} \\ b_{\mathbf{q}}^\dagger \end{pmatrix} \ , \tag{2.3}$$

where

$$b_{\mathbf{q}}^\dagger = \frac{1}{\sqrt{N}} \sum_i e^{-i\mathbf{q}\cdot\mathbf{R}_i} a_i^\dagger \ , \quad b_{\mathbf{q}} = \frac{1}{\sqrt{N}} \sum_i e^{i\mathbf{q}\cdot\mathbf{R}_i} a_i \ , \tag{2.4}$$

$$\begin{aligned} u_{\mathbf{q}} &= \sqrt{\frac{1+\sqrt{1-\kappa^2\gamma_{\mathbf{q}}^2}}{2\sqrt{1-\kappa^2\gamma_{\mathbf{q}}^2}}} \ , \\ v_{\mathbf{q}} &= -\mathrm{sgn}(\gamma_{\mathbf{q}}) \sqrt{\frac{1-\sqrt{1-\kappa^2\gamma_{\mathbf{q}}^2}}{2\sqrt{1-\kappa^2\gamma_{\mathbf{q}}^2}}} \ , \\ \gamma_{\mathbf{k}} &= \frac{1}{z} \sum_{j=1}^{z} e^{i\mathbf{k}\cdot\mathbf{R}_j} \ , \end{aligned} \tag{2.5}$$

and

$$[a_i, a_j^\dagger] = \delta_{ij} \Longleftrightarrow [\alpha_{\mathbf{q}}, \alpha_{\mathbf{q}'}^\dagger] = \delta_{\mathbf{q}\mathbf{q}'} \ , \tag{2.6}$$

$z$ representing the number of nearest neighbors. Taking into account only interaction terms linear in magnon variables we get the basic fermion-magnon Hamiltonian[11,14]

$$\begin{aligned} \mathcal{H}_{\mathrm{I}} = & \sum_{\mathbf{k}s} \varepsilon_{\mathbf{k}} c_{\mathbf{k}s}^\dagger c_{\mathbf{k}s} + \sum_{\mathbf{q}} \omega_{\mathbf{q}} \alpha_{\mathbf{q}}^\dagger \alpha_{\mathbf{q}} + \tfrac{1}{4} V_{\parallel} \sum_{\mathbf{k}s} c_{\mathbf{k}-\mathbf{q}_0 s}^\dagger c_{\mathbf{k}s} \sigma_{ss}^z \\ & + \frac{1}{\sqrt{N}} \sum_{\mathbf{k}\mathbf{q}ss'} \tfrac{1}{4}(u_{\mathbf{q}} + v_{\mathbf{q}})[V_\perp + z t_1(\gamma_{\mathbf{k}} + \gamma_{\mathbf{k}-\mathbf{q}})] \\ & \times [c_{\mathbf{k}-\mathbf{q}s}^\dagger c_{\mathbf{k}s'}(\sigma_{ss'}^x \alpha_{\mathbf{q}}^\dagger + i\sigma_{ss'}^y \alpha_{\mathbf{q}+\mathbf{q}_0}^\dagger) + c_{\mathbf{k}s}^\dagger c_{\mathbf{k}-\mathbf{q}s'}(\sigma_{ss'}^x \alpha_{\mathbf{q}} - i\sigma_{ss'}^y \alpha_{\mathbf{q}+\mathbf{q}_0})] \end{aligned} \tag{2.7}$$

with $\omega_{\mathbf{q}} = \frac{1}{2} z J \sqrt{1-\kappa^2\gamma_{\mathbf{q}}^2}$ and $\varepsilon_{\mathbf{k}} = -z t_0 \gamma_{\mathbf{k}}$. In the following we assume $z=4$ as for the square two-dimensional (2D) lattice. In Eq. (2.7) we have separated the Kondo term into a longitudinal $V_{\parallel}$ contribution and the spin-flip $V_\perp$ contribution in order to enable later the expansion in $V_\perp$.

In $\mathcal{H}_{\mathrm{I}}$ (2.7) the free $t_0$ hopping is diagonal, while the spin-dependent hopping $t_1$ term is off diagonal in spin variables. Since $t_1$ seems to be dominant[10] even in the relevant parameter regime for $CuO_2$ layers, it is convenient also to introduce the staggered fermionic operators $\tilde{c}_{i\sigma}^\dagger, \tilde{c}_{i\sigma}$, e.g.,

$$\begin{aligned} \tilde{c}_{i\sigma}^\dagger &= \sum_{\sigma} \tfrac{1}{2}(1 + 4\sigma s e^{i\mathbf{q}_0\mathbf{R}_i}) c_{is}^\dagger \ , \\ \tilde{c}_{\mathbf{k}\pm}^\dagger &= \tfrac{1}{2}[(c_{\mathbf{k}+}^\dagger + c_{\mathbf{k}-}^\dagger) \pm (c_{\mathbf{k}+\mathbf{q}_0+}^\dagger - c_{\mathbf{k}+\mathbf{q}_0-}^\dagger)] \ , \end{aligned} \tag{2.8}$$

where we used $\pm$ for $s = \pm\frac{1}{2}$ and $\sigma = \pm\frac{1}{2}$. So an alternative model $\mathcal{H}_{\mathrm{II}}$ in terms of transformed $\tilde{c}_{\mathbf{k}\sigma}$ appears to be

$$\mathcal{H}_{\rm II} = \sum_{\mathbf{k}\sigma\sigma'} (\varepsilon_{\mathbf{k}} \sigma^x_{\sigma\sigma'} + \tfrac{1}{4} V_{\parallel} \sigma^z_{\sigma\sigma'}) \tilde{c}^{\dagger}_{\mathbf{k}\sigma} \tilde{c}_{\mathbf{k}\sigma'} + \sum_{\mathbf{q}} \omega_{\mathbf{q}} \alpha^{\dagger}_{\mathbf{q}} \alpha_{\mathbf{q}} + \frac{1}{\sqrt{N}} \sum_{\mathbf{k}\mathbf{q}\sigma\sigma'} U_{\sigma\sigma'}(\mathbf{k},\mathbf{q}) (\tilde{c}^{\dagger}_{\mathbf{k}-\mathbf{q}\sigma} \tilde{c}_{\mathbf{k}\sigma'} \alpha^{\dagger}_{\mathbf{q}} + \tilde{c}^{\dagger}_{\mathbf{k}\sigma'} \tilde{c}_{\mathbf{k}-\mathbf{q}\sigma} \alpha_{\mathbf{q}}) \ , \tag{2.9}$$

with

$$U(\mathbf{k},\mathbf{q}) = \begin{pmatrix} \frac{1}{2} z t_1 (\gamma_{\mathbf{k}} u_{\mathbf{q}} + \gamma_{\mathbf{k}-\mathbf{q}} v_{\mathbf{q}}) & \frac{1}{2} V_{\perp} u_{\mathbf{q}} \\ \frac{1}{2} V_{\perp} v_{\mathbf{q}} & \frac{1}{2} z t_1 (\gamma_{\mathbf{k}} v_{\mathbf{q}} + \gamma_{\mathbf{k}-\mathbf{q}} u_{\mathbf{q}}) \end{pmatrix} = \begin{pmatrix} U_+ & U_{+-} \\ U_{-+} & U_- \end{pmatrix} . \tag{2.10}$$

Here the $t_1$ hopping is diagonal in new ($\sigma$) spin variables. Relative to the importance of $t_0$ and $t_1$ hopping we shall in the following use either $\mathcal{H}_{\rm I}$ or $\mathcal{H}_{\rm II}$ models as the starting model.

## III. PERTURBATION EXPANSION

### A. Self-energy of a mobile fermion

Let us first consider the $T$=0 self-energy $\Sigma(\mathbf{k},\omega)$ of a fermion in the model (1.1) with the free hopping only, i.e., $t_0 \neq 0$, $t_1$=0. We perform the perturbation expansion for $\mathcal{H}_{\rm I}$ assuming $V_{\perp} \ll t_0, J$. Here we omit $V_{\parallel}$, since it is not essential for low-$\omega$ behavior in this regime.

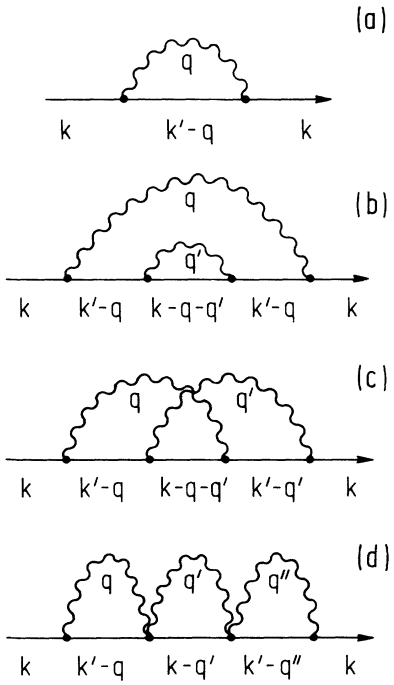


FIG. 1. The second- (a) and fourth- (b) and (c) order diagrams in $V_{\perp}$ expansion. Diagram (d) is one of the representatives for the nonlinear $V_{\parallel}$ coupling.

To the lowest order in $V_{\perp}$ the $\Sigma(\mathbf{k},\omega)$ is determined by the process, presented in Fig. 1(a),

$$\Sigma(\mathbf{k},\omega) = \frac{2}{(8\pi)^2} \int d^2q \frac{V_{\perp}^2 (u_{\mathbf{q}} + v_{\mathbf{q}})^2}{\varepsilon_0 + \omega - \varepsilon_{\mathbf{k}-\mathbf{q}} - \omega_{\mathbf{q}}} \ . \tag{3.1}$$

Here we take $\varepsilon_0 = \varepsilon_{\mathbf{k}=0}$, and hence we measure $\omega$ from the bottom of the unperturbed band. In all further calculations we assume $\mathrm{Im}\,\omega = \eta \to 0^+$. The binding energy $\varepsilon_b$ of the spin polaron, having $k = 0$ ground state in the $t_1 = 0$ model, is given by $\Sigma(0,0)$. It has been evaluated in Ref. (11) and shown to be finite. On the other hand, for $\mathbf{k} = \mathbf{q}_0$, $\Sigma(\mathbf{k},\omega)$ has a singular behavior at the low-frequency edge $\omega \sim 0$,

$$\Sigma(\mathbf{q}_0,\omega) \sim \frac{V_{\perp}^2}{J} \ln(-\omega/J) \ , \tag{3.2}$$

where $\ln(-\omega) = \ln|\omega| - i\pi\Theta(\omega)$. The singularity in Eq. (3.2) appears due to the coupling $u_{\mathbf{q}} + v_{\mathbf{q}} \sim |\mathbf{q} - \mathbf{q}_0|^{-1/2}$, divergent at $\mathbf{q} \to \mathbf{q}_0$.

It can be shown that also higher-order processes, as in Figs. 1(b) and 1(c), do not yield a diverging $\varepsilon_b$ within $\mathcal{H}_{\rm I}$. Let us therefore comment on the recent analysis by Furukawa and Imada.[14] They consider the effect of the nonlinear term, originating from Eq. (2.2), which has in our notation the form

$$\mathcal{H}_{\rm I}^{(2)} = -V_{\parallel} \frac{1}{N} \sum_{\mathbf{k}\mathbf{q}\mathbf{q}'s} s(u_{\mathbf{q}} u_{\mathbf{q}'} + v_{\mathbf{q}} v_{\mathbf{q}'}) c^{\dagger}_{\mathbf{k}+\mathbf{q}_0-\mathbf{q},s} c_{\mathbf{k}-\mathbf{q}',s} \times [\alpha^{\dagger}_{\mathbf{q}} \alpha_{\mathbf{q}'} + \tfrac{1}{2}(\alpha^{\dagger}_{\mathbf{q}} \alpha^{\dagger}_{-\mathbf{q}'} + \alpha_{-\mathbf{q}} \alpha_{\mathbf{q}'})] \ . \tag{3.3}$$

It is argued[14] that these terms cause divergencies in $\varepsilon_b$, i.e., an expansion of $\varepsilon_b$ in $V_{\parallel}$ is singular due to graphs of the type presented in Fig. 1(d). In the Appendix we perform the summation of the most divergent terms involving at most a single magnon excitation in the intermediate state. It yields merely a renormalization of the QP parameters, leaving $\varepsilon_b > 0$ and finite. We are interested mainly in $\omega \approx 0$ behavior at fixed $V_{\perp}$. In this respect we expect that the $\omega \approx 0$ regime will still be governed by $u_{\mathbf{q}\to 0}$ divergencies, which remain unrenormalized. In

the following analysis we therefore neglect the nonlinear term, Eq. (3.3).

Let us now evaluate higher-order contributions to the QP excitation spectra, as determined by the $\Sigma''(\mathbf{k},\omega)$. Due to the linear dispersion $\omega_{\mathbf{q}} \sim \sqrt{2}Jq \equiv c_0 q$ for $q \to 0$ and $\omega_{\mathbf{q}} \sim c_0|\mathbf{q}-\mathbf{q}_0|$ for $\mathbf{q} \to \mathbf{q}_0$, long-wavelength magnons will dominate the small $\omega$ regime. The most important part in $\mathcal{H}_{\mathrm{I}}$ is thus at $\mathbf{q} \to \mathbf{q}_0$:

$$\mathcal{H}_{\mathrm{I}} \sim V_\perp \sum_{\mathbf{k}ss'} \sum_{\mathbf{q}\sim\mathbf{q}_0} \frac{1}{\sqrt{|\mathbf{q}-\mathbf{q}_0|}} c^\dagger_{\mathbf{k}-\mathbf{q},s} c_{\mathbf{k}s'} \times [\sigma^x_{ss'}(\alpha^\dagger_{\mathbf{q}} + \alpha_{-\mathbf{q}}) + i\sigma^y_{ss'}(\alpha^\dagger_{\mathbf{q}_0+\mathbf{q}} - \alpha_{-\mathbf{q}_0-\mathbf{q}})] \,. \tag{3.4}$$

The lowest-order nontrivial terms in $\Sigma(\mathbf{k},\omega)$ correspond to diagrams in Figs. 1(b) and 1(c),

$$\Sigma(\mathbf{k},\omega) = \frac{4}{(8\pi)^4} \int d^2q \int d^2q' \frac{V_\perp^4 (u_{\mathbf{q}}+v_{\mathbf{q}})^2 (u_{\mathbf{q}'}+v_{\mathbf{q}'})^2}{\varepsilon_0+\omega-\varepsilon_{\mathbf{k}-\mathbf{q}}-\omega_{\mathbf{q}}} \left( \frac{1}{\varepsilon_0+\omega-\varepsilon_{\mathbf{k}-\mathbf{q}}-\omega_{\mathbf{q}}} + \frac{1}{\varepsilon_0+\omega-\varepsilon_{\mathbf{k}-\mathbf{q}'}-\omega_{\mathbf{q}'}} \right) \times \frac{1}{\varepsilon_0+\omega-\varepsilon_{\mathbf{k}-\mathbf{q}-\mathbf{q}'}-\omega_{\mathbf{q}}-\omega_{\mathbf{q}'}} \,. \tag{3.5}$$

We note from Eq. (3.5) that the noncrossing diagrams (first term) and the crossing diagrams (second term) yield the same contribution to the singular behavior at $\omega \gtrsim 0$. Both contributions add at $k=0$, and we get

$$\Sigma(0,\omega) \sim V_\perp^4 \int d^2q \int d^2q' \frac{|\mathbf{q}|^{-1}\,|\mathbf{q}'|^{-1}}{(\omega-8t_0)^2} \frac{1}{\omega-\omega_{\mathbf{q}}-\omega_{\mathbf{q}'}} \sim \frac{V_\perp^4}{t_0^2} \int dq \int dq' \frac{1}{\omega - c_0(q+q')} \,, \tag{3.6}$$

where we consider only the most singular part (3.4). We assume also a large width $8t_0$ of the free particle band, i.e., $8t_0 \gg J$. We thus get at small frequencies $|\omega| \ll J$

$$\Sigma(0,\omega) \sim \frac{V_\perp^4}{t_0^2 J^2} \omega \ln(-\omega/J) \,. \tag{3.7}$$

Hence, the low-excitation part of the QP spectra appears to be nonanalytical with $\Sigma''(0,\omega>0) \sim \omega$. It should be noted that in the analogous treatment of the $t$-$J$ model,[3,4] the local coupling (the local constraint) is not taken into account and therefore the low-frequency anomaly does not appear, i.e., $\Sigma''(0,\omega>0) \lesssim \omega^2$.

We do not investigate here systematically higher-order corrections to Eq. (3.7), leading mainly to energy shifts of the QP band. We estimate only the most singular contributions of higher-order diagrams yielding logarithmic corrections to $\Sigma''$,

$$\Sigma''(0,\omega>0) \sim \omega \left[ 1 + c_1 \frac{V_\perp^2}{t_0 J} \ln(\omega/J) + c_2 \left( \frac{V_\perp^2}{t_0 J} \ln(\omega/J) \right)^2 + \cdots \right] , \tag{3.8}$$

where $c_i$ are numerical constants. Clearly, the consideration of higher terms is essential for small frequencies $\omega < \omega_c \sim J \exp(-t_0 J/V_\perp^2)$.

Spin-dependent hopping terms ($t_1$) are not singular at $\mathbf{q} \to \mathbf{q}_0$, since the coupling is of the gradient type for $\mathbf{q} \sim \mathbf{q}_0$,

$$t_1|\gamma_{\mathbf{k}} + \gamma_{\mathbf{k}-\mathbf{q}}| = t_1|\gamma_{\mathbf{k}} - \gamma_{\mathbf{k}+\mathbf{q}_0-\mathbf{q}}| \sim t_1|(\mathbf{q}-\mathbf{q}_0)\cdot\nabla\gamma_{\mathbf{k}}| \le t_1|\mathbf{q}-\mathbf{q}_0| \,. \tag{3.9}$$

The $t_1$ term does not contribute to $\Sigma''$ at low $\omega$ as does the local $V$ term, and consequently does not lead to the singular behavior as in Eq. (3.7). The low excitation spectrum of QP is thus dominated by the local Kondo $V_\perp$ term.

A direct consequence of the nonanalytical behavior of $\Sigma(\omega)$ is the disappearance of the well-defined peak at the bottom of the QP spectra, which should show up in the form

$$G(\mathbf{k},\omega) = \frac{a_{\mathbf{k}}}{\omega-\omega_{\mathbf{k}}} + \tilde{G}(\mathbf{k},\omega) \,, \tag{3.10}$$

while in our case

$$a_{\mathbf{k}} = \left( 1 - \left. \frac{\partial\Sigma(\mathbf{k},\omega)}{\partial\omega} \right|_{\omega=0} \right)^{-1} \to 0 \quad \text{as} \quad \mathbf{k} \to 0 \,. \tag{3.11}$$

### B. Localized fermion

The same perturbation treatment of $\mathcal{H}_{\mathrm{I}}$ cannot be applied if the fermion is localized, i.e., for $t_0 = t_1 = 0$, since the self-energy appears to be divergent even within the lowest order in $V$, as in Eq. (3.1).

Fermion-magnon Hamiltonian $\mathcal{H}_{\mathrm{II}}$, expressed in staggered fermion basis, can still be treated perturbatively if we take $V_\perp$ and $V_\parallel$ as independent parameters. The small parameter is then $V_\perp/V_\parallel < 1$. Low-order processes still correspond to those in Fig. 1, where we replace $\varepsilon_{\mathbf{k}}$ with either $\varepsilon_0$ for $\sigma = -\frac{1}{2}$ or $\varepsilon_0 + \frac{1}{2}V_\parallel$ for $\sigma = +\frac{1}{2}$. We choose $\varepsilon_0 = -\frac{1}{4}V_\parallel$ being the unperturbed fermion energy in this case.

Within the lowest order, analogous to Eq. (3.1), the energy of the localized singletlike $\sigma = -\frac{1}{2}$ state is given by

$$\varepsilon_b = \varepsilon_0 - \frac{V_\perp^2}{(4\pi)^2}\int d^2q \frac{|u_\mathbf{q}|^2}{\frac{1}{2}V_\parallel + \omega_\mathbf{q}} \sim \varepsilon_0 - 0.598\,\frac{V_\perp^2}{V_\parallel}\ , \qquad J/V_\parallel \ll 1\ . \quad (3.12)$$

$\varepsilon_b$ corresponding to the $\sigma = -\frac{1}{2}$ state is thus nonsingular, while higher-state self-energy $\Sigma_+$ again shows in the lowest order the logarithmic divergence analogous to Eq. (3.2),

$$\Sigma_+(\omega) \sim \frac{V_\perp^2}{J}\ln(-\omega/J), \qquad |\omega| \ll J\ . \quad (3.13)$$

As in Sec. III A we can calculate fourth-order corrections corresponding to diagrams in Figs. 1(b) and 1(c),

$$\Sigma_-(\omega) = \frac{2}{(4\pi)^4}\int d^2q \int d^2q' \frac{V_\perp^4}{(\omega - \omega_\mathbf{q} - \omega_{\mathbf{q}'})(\omega - \frac{1}{2}V_\parallel - \omega_\mathbf{q})}\left(\frac{(u_\mathbf{q}v_{\mathbf{q}'})^2}{\omega - \frac{1}{2}V_\parallel - \omega_\mathbf{q}} + \frac{u_\mathbf{q}v_\mathbf{q}\,u_{\mathbf{q}'}v_{\mathbf{q}'}}{\omega - \frac{1}{2}V_\parallel - \omega_{\mathbf{q}'}}\right)\ . \quad (3.14)$$

The second term in Eq. (3.14)—corresponding to crossing diagrams—vanishes identically due to symmetry of the function $u_\mathbf{q}v_\mathbf{q}$, Eq. (2.5). From the noncrossing diagrams (first term) we again get the nonanalytical behavior of the form (3.7),

$$\Sigma_-(\omega) \sim \frac{V_\perp^4}{V_\parallel^2 J^2}\omega\ln(-\omega/J)\ . \quad (3.15)$$

We can thus conclude that the anomalous behavior appears in both cases, i.e., for the mobile fermion and for the localized fermion. It has a common origin in the singular interaction term $V_\perp\frac{1}{\sqrt{q}}$ that couples $c_{\mathbf{k}s}$ with $c_{\mathbf{k}+\mathbf{q}_0 s'}$ in $\mathcal{H}_\mathrm{I}$ or $\tilde{c}_{\mathbf{k}-}$ with $\tilde{c}_{\mathbf{k}+}$ in $\mathcal{H}_\mathrm{II}$, respectively.

## IV. SELF-CONSISTENT EQUATIONS

In this section we generalize the self-consistent (SC) method, as followed by Kane *et al.*,[4] to our coupled fermion-magnon model. We choose the free part in $\mathcal{H}_\mathrm{II}$, Eq. (2.9), as

$$\mathcal{H}_\mathrm{II}^0 = \sum_{\mathbf{k}\sigma\sigma'}(\varepsilon_\mathbf{k}\sigma^x_{\sigma\sigma'} + \tfrac{1}{4}V_\parallel\sigma^z_{\sigma\sigma'})\tilde{c}^\dagger_{\mathbf{k}\sigma}\tilde{c}_{\mathbf{k}\sigma'} \quad (4.1)$$

with the corresponding Green's function

$$G_0(\mathbf{k},\omega) = (\omega - \mathcal{H}_\mathrm{II}^0)^{-1} = \begin{pmatrix} \omega - \frac{1}{4}V_\parallel & -\varepsilon_\mathbf{k} \\ -\varepsilon_\mathbf{k} & \omega + \frac{1}{4}V_\parallel \end{pmatrix}^{-1}\ . \quad (4.2)$$

SC equations for the fermion self-energy, which emerge from a summation of noncrossing diagrams as in Figs. 1(a) and 1(b) to all orders, can be written as

$$\Sigma_{\sigma\sigma'}(\mathbf{k},\omega) = \sum_{\tau\tau'}\frac{1}{(2\pi)^2}\int d^2q\, \mathcal{U}_{\tau\sigma}(\mathbf{k},\mathbf{q})G_{\tau\tau'}(\mathbf{k}-\mathbf{q},\omega-\omega_\mathbf{q})\mathcal{U}_{\tau'\sigma'}(\mathbf{k},\mathbf{q})\ , \quad (4.3)$$

where the fermion propagator $G(\mathbf{k},\omega)$ is given by

$$G(\mathbf{k},\omega) = [G_0^{-1}(\mathbf{k},\omega) - \Sigma(\mathbf{k},\omega)]^{-1} = \begin{pmatrix} G_+ & G_{+-} \\ G_{-+} & G_- \end{pmatrix} \quad (4.4)$$

and

$$\Sigma(\mathbf{k},\omega) = \begin{pmatrix} \Sigma_+ & \Sigma_{+-} \\ \Sigma_{-+} & \Sigma_- \end{pmatrix}\ . \quad (4.5)$$

It should be stressed that in our SC approach, as well as in the approach by Kane *et al.*, all contributions from crossing diagrams are neglected, although we cannot exclude the possibility that these contributions would modify the low-frequency anomalies.

### A. Localized fermion

Let us investigate first SC Eqs. (4.3)–(4.5) for a localized fermion coupled to the AFM background only via the local $V$ term. Eq. (4.3) is in this case independent on $\mathbf{k}$ and simplifies to

$$\Sigma_\pm(\omega) = \frac{1}{(2\pi)^2}\int d^2q\,|\mathcal{U}_{\pm\mp}|^2 G_\mp(\omega - \omega_\mathbf{q}) \quad (4.6)$$

with

$$G_\pm(\omega) = \frac{1}{\omega \mp \frac{1}{4}V_\parallel - \Sigma_\pm(\omega)}\ . \quad (4.7)$$

#### 1. Ising limit

Equations (4.6) become trivial in the *Ising* limit, where $\kappa$=0 and thus $u_\mathbf{q}$=1, $v_\mathbf{q}$=0, and $\omega_\mathbf{q} = 2J$. Since the SC equations make sense for arbitrary parameters $V_\perp, V_\parallel$ we study in the following only the most interesting isotropic case with $V = V_\perp = V_\parallel$. From Eq. (4.6) it follows that $\Sigma_+$=0; hence the function $G_+$ has a single pole at $\omega = \frac{1}{4}V$. This pole thus corresponds approximately to the triplet state. On the other hand we get for $\Sigma_-$

$$\Sigma_-(\omega) = \tfrac{1}{4}V^2 G_+(\omega - 2J) = \frac{\frac{1}{4}V^2}{\omega - \frac{1}{4}V - 2J} , \tag{4.8}$$

so that

$$G_-(\omega) = \left(\omega + \tfrac{1}{4}V - \frac{\frac{1}{4}V^2}{\omega - \frac{1}{4}V - 2J}\right)^{-1} = \frac{a}{\omega - \omega_<} + \frac{1-a}{\omega - \omega_>} . \tag{4.9}$$

The meaning of both poles can be easily recognized from the limit $J/V \to 0$, where we get $\omega_{\gtrless} = \pm\frac{\sqrt{5}}{4}V$, while the strength of the lower pole is $a = \frac{1+\sqrt{5}}{2\sqrt{5}} \approx 0.72$. The lower pole can be attributed to the local singlet, while the upper pole belongs to the triplet state. Note that the correct result for the local singlet and triplet should be $\omega_< = -\frac{3}{4}V$, $\omega_> = \frac{1}{4}V$, and $a = \frac{1}{2}$. Due to the linearization of spin operators in Eq. (2.9) analysis thus fails to reproduce all quantitative aspects of local singlets. Still the description is qualitatively correct. In particular we do not expect that these deviations would have any effect on singular low-$\omega$ behavior.

In the intermediate region between the Ising limit and the isotropic Heisenberg case we can get a reasonable approximation by neglecting the dispersion in $\omega_q \sim \bar{\omega} = 2J(1-\frac{1}{2}\kappa^2)$, while retaining it in $|v_q|^2 \sim \frac{1}{4}\kappa^2\gamma_q^2$. Equations (4.6) can be then written as

$$\Sigma_+(\omega) = \tfrac{1}{4}V^2 G_-(\omega - \bar{\omega})y ,$$
$$\Sigma_-(\omega) = \tfrac{1}{4}V^2 G_+(\omega - \bar{\omega})(1+y) \tag{4.10}$$

with

$$y = \frac{1}{(2\pi)^2}\int |v_q|^2 d^2q \sim \frac{\kappa^2}{16} . \tag{4.11}$$

Note that Eqs. (4.10) are a valid approximation of (4.3) only for $\kappa < 1$. As a solution of coupled set (4.10) we get a set of isolated poles,

$$G_-(\omega) = \sum_i \frac{a_i}{\omega - \omega_i} , \tag{4.12}$$

where

$$\omega_{i+1} - \omega_i = \Delta_i \sim V\left(\frac{J}{V}\right)^{\frac{2}{3}} , \qquad a_i \sim \frac{J}{V} \tag{4.13}$$

for small $i$ and fixed $\kappa < 1$ in the limit $J/V \ll 1$. In the limit $\kappa \to 0$ only two poles remain; see Eq. (4.9). Finite $\kappa < 1$ induces the coupling of neighboring spins via $S_i^+ S_j^-$ term in (1.1) what causes the spreading of the strength $a$ at $\omega = \omega_<$ and $1-a$ at $\omega = \omega_>$ into two sets of isolated states centered around $\omega_<$ and $\omega_>$, respectively. In Fig. 2 we show the lower (singletlike) part of the spectral function $A_-(\omega)$ for $J/V$=0.01 as a set of lines, where the height of each represents the strength $a_i$ and $\sum_i a_i$=0.72. Equations (4.10) were solved using $y(\kappa = 1) = 0.196$ and $\bar{\omega} \equiv J$.

It is interesting to investigate the limit $J \to 0^+$. In this case the distances between the poles in Eq. (4.12) approach zero and the result is a broad spectrum. The exact solution for the self-energy is then

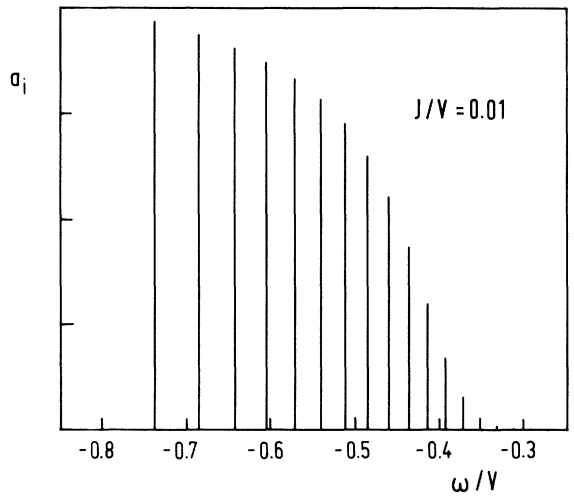


FIG. 2. Spectral function $A_-(\omega)$ vs $\omega/V$ presented as a set of lines with the strength $a_i$ normalized to $\sum_i a_i = 0.72$. The calculation was performed at $J/V = 0.01$ using $y = 0.196$ and $\bar{\omega} = J$.

$$\Sigma_\pm(\omega) = \frac{\zeta \mp \frac{1}{4}V^2 - \sqrt{(\zeta - \zeta_1)(\zeta - \zeta_2)}}{2(\omega \pm \frac{1}{4}V)} , \tag{4.14}$$

$$\zeta = \omega^2 - (\tfrac{1}{4}V)^2 , \quad \zeta_{1,2} = \tfrac{1}{4}V^2(1 + 2y \pm \sqrt{y^2 + y}) \tag{4.15}$$

with the spectral functions

$$A_-(\omega) = -\frac{1}{\pi}\mathrm{Im}G_-(\omega) = \frac{2\sqrt{(\omega_1^2 - \omega^2)(\omega^2 - \omega_2^2)}}{\pi y V^2 |\omega + \frac{1}{4}V|} ,$$
$$\omega_2^2 \le \omega^2 \le \omega_1^2 , \tag{4.16}$$
$$A_+(\omega) = \frac{y}{1+y}A_-(-\omega) + \frac{1}{1+y}\delta(\omega - \tfrac{1}{4}V) .$$

Here, $y$ and $\omega_{1,2}$ still depend on $\kappa$. In the Ising limit $\kappa \to 0$ the result (4.9) again reappears from Eq. (4.16). Approaching the isotropic case $\kappa$=1 we get $\omega_1 = \pm 0.808\,V$, $\omega_2 = \pm 0.410\,V$. In Fig. 3 we plot $A_-(\omega)$, consisting of two separated areas centered around $\omega \sim \pm\frac{\sqrt{5}}{4}V$. The total weight of the lower ("singlet") part, $\int_{\omega_1}^{\omega_2} A_-(\omega)d\omega$, is still equal to $a$=0.72.

The spectral function $A_+(\omega)$, also presented in Fig. 3, consists of three areas, two centered around $\omega \sim \pm\frac{\sqrt{5}}{4}V$ and with one pole at $\omega = \frac{1}{4}V$. For the orientation we also present in Fig. 3 positions and the relative strength

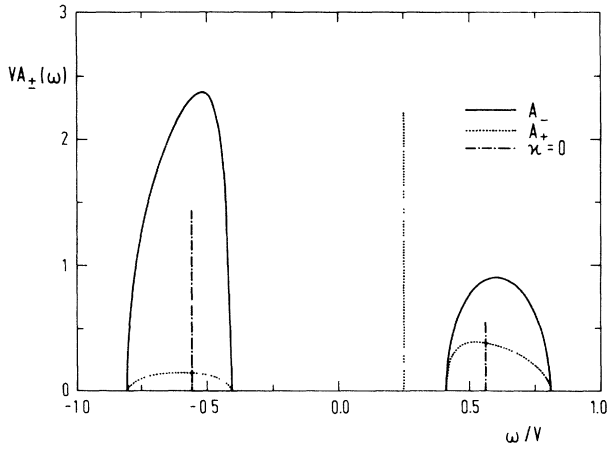


FIG. 3. "Singlet" and "triplet" spectral functions $VA_{\pm}(\omega)$ vs $\omega/V$ both for the limit $J = 0^+$. Dash-dotted lines show the Ising limit ($\kappa = 0$) result.

of poles in (4.9) for $J/V \to 0$. Using the result (4.16) one can also qualitatively reproduce relations (4.13) by applying the isolated pole approximation to $G(\omega)$ as Kane *et al.*[4]

### 2. Heisenberg case

The behavior of the isotropic model $\kappa=1$ is qualitatively different from the previous anisotropic cases due to the disappearance of the magnon gap, i.e., $\omega_q \sim c_0 q$. A consequence of the divergent coupling of the fermion with low-frequency magnons are anomalies observed already in the perturbative treatment, Sec. III. Equations (4.6) now allow for a study of low-frequency behavior beyond the perturbative regime. It should be also noted that the present problem of the localized fermion coupled with magnons is identical to that of a pseudospin (two-level system) interacting with a phonon bath via a piezoelectrictype coupling.[15]

For small $V_\perp/V_\parallel$ Eqs. (4.6) reproduce perturbative results in the regime $\omega > \omega_c \sim J\exp(-JV_\parallel/V_\perp^2)$. Novel results are, however, obtained for $\omega < \omega_c$. In this regime the most important is the long-wavelength part of $\mathcal{H}_{II}$, analogous to Eq. (3.4),

$$\mathcal{H}_{II} \sim V_\perp \sum_{\mathbf{k},\sigma\sigma'} \left( \sum_{\mathbf{q}\sim 0} \frac{1}{\sqrt{q}} \tilde{c}^\dagger_{\mathbf{k}-\mathbf{q},\sigma} \tilde{c}_{\mathbf{k}\sigma'} \frac{1}{i} \sigma^y_{\sigma\sigma'} (\alpha^\dagger_{\mathbf{q}} - \alpha_{-\mathbf{q}}) + \sum_{\mathbf{q}\sim\mathbf{q}_0} \frac{1}{\sqrt{|\mathbf{q}-\mathbf{q}_0|}} \tilde{c}^\dagger_{\mathbf{k}-\mathbf{q},\sigma} \tilde{c}_{\mathbf{k}\sigma'} \sigma^x_{\sigma\sigma'} \times (\alpha^\dagger_{\mathbf{q}} + \alpha_{-\mathbf{q}}) \right) . \quad (4.17)$$

Hence, Eq. (4.6) reduces to

$$\Sigma_\pm(\omega) = \frac{\sqrt{2}V^2}{8\pi^2} \int \frac{dq}{\omega \mp \frac{1}{4}V - c_0 q - \Sigma_\mp(\omega - c_0 q)} . \quad (4.18)$$

Two Eqs. (4.18) can be now solved analytically for $\tilde{\omega} \ll \omega_c$, where we have denoted $\tilde{\omega} = \omega - \omega_0$ as the energy difference from the bottom of the spectrum. The solution can be obtained by inserting into Eq. (4.18) an ansatz $\Sigma_\pm(\omega) \sim b_\pm(-\tilde{\omega})^{\alpha_\pm}$. We observe that the only consistent values for $\alpha$ are $\alpha_- = 1 - \alpha_+ = \frac{1}{2}$. So the behavior for $\tilde{\omega} \to 0^+$ appears to be

$$A_\pm(\omega) = \frac{1}{\pi b_\pm \sqrt{\tilde{\omega}}} , \qquad b_+ b_- = \frac{1}{4\pi}\frac{V^2}{J} . \quad (4.19)$$

Note that the ratio $A_-/A_+ = b_+/b_-$ is a constant for small $\tilde{\omega}$.

The SC Eqs. (4.3) can be solved numerically. From their structure it is evident that $\Sigma_\pm(\omega_1)$ is easily obtained if $\Sigma_\pm(\omega)$ is known for all $\omega_1 - 2J < \omega < \omega_1$. From Eq. (4.3) it is also clear that $\Sigma_\pm \to 0^-$ for $\omega \to -\infty$. Our numerical procedure thus consists of two parts: We first calculate $\Sigma_\pm(\omega)$ at $\omega \ll 0$ using in Eq. (4.3) $G_0(\omega)$ instead of $G(\omega)$. Then $\Sigma_\pm(\omega)$ are subsequently evaluated from previous values $\Sigma_\pm(\omega - \omega_q)$. It turns out that such a procedure is very stable with enough energy mash points in $\Sigma_\pm(\omega)$.

In Fig. 4, $\Sigma''_-(\omega)$ is presented for three different values of $V/J$. For $V/J=2.5$ we see a linear energy dependence similar to Eq. (3.15) except at very low $\tilde{\omega}$ where, according to Eq. (4.19), $\Sigma''_-(\omega) \sim \sqrt{\tilde{\omega}}$. This square-root dependence becomes more pronounced at $V/J > 10$.

In Figs. 5 and 6 we show $A_+(\omega)$ and $A_-(\omega)$ corresponding to $\Sigma$ from Fig. 4. In both regimes, i.e., of small and large $V/J$, the lower edge of the spectrum is dominated

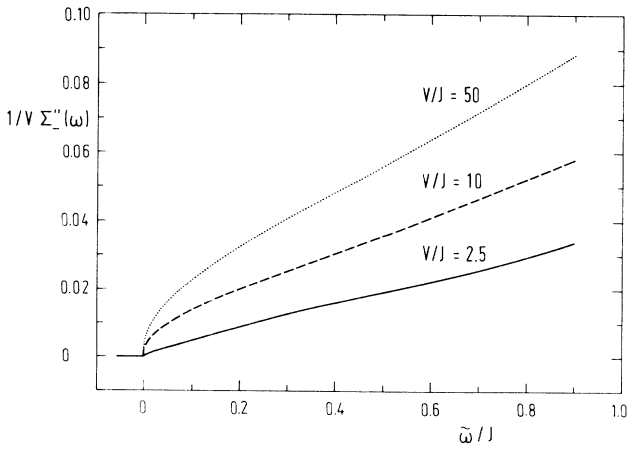


FIG. 4. $\Sigma''_-(\omega)/V$ vs $\tilde{\omega}/J$ for three values of $V/J$.

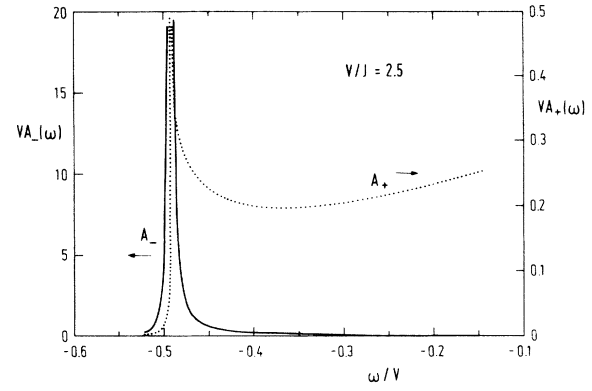


FIG. 5. Spectral functions $V A_{\pm}(\omega)$ vs $\omega/V$ for $V/J$=2.5. Note different scales for $A_+$ and $A_-$.

by a QP peak, which is not a $\delta$ function. This is evident from the asymmetry due to $\Sigma_-''(\tilde{\omega} > 0) \approx \tilde{\omega}$. $A_+(\omega)$ shows in both cases a $1/\sqrt{\tilde{\omega}}$ shape. At $V/J = 2.5$, $A_+(\omega)$ is nearly constant for larger $\omega$. For large $V/J = 50$ in Fig. 6 both $A_+(\omega)$ and $A_-(\omega)$ have the same qualitative behavior with more structure, while the constant $b_+/b_-$ is in agreement with Eq. (4.16). Analysis of the distance between the peaks in the latter case shows again $(J/V)^{2/3}$ dependence. In Fig. 6 we also present for comparison the $J/V \to 0^+$ limit (4.16) for $A_-(\omega)$. The agreement between this limiting shape and the calculated $A_-(\omega)$ appears even more pronounced at higher $V/J$. Simplified set of Eqs. (4.10) is thus a good approximation Eq. (4.3) also in the Heisenberg case if only $\tilde{\omega}$ is not too close to the bottom of the spectrum.

We have in this section restricted ourselves to the case of a localized fermion, but the result obtained in Eq. (4.19) holds also for $t_0 \neq 0$. For the latter case we obtain from $\mathcal{H}_I$ SC equations analogous to Eqs. (4.18), but replacing $\frac{1}{2}V$ with $8t_0$ in the denominator.

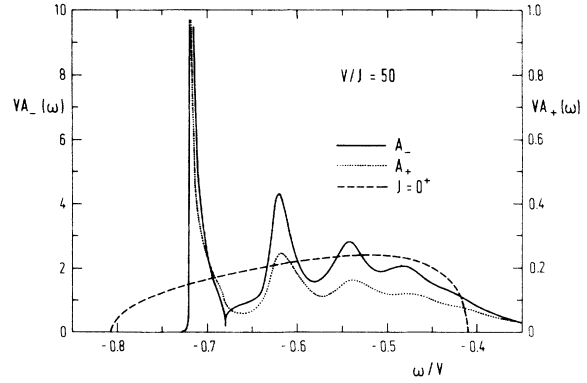


FIG. 6. Spectral functions $V A_{\pm}(\omega)$ vs $\omega/V$ for $V/J$=50. Dashed line represents $J = 0^+$ limit for $A_-(\omega)$.

### B. Mobile quasiparticle

Although the properties of a mobile fermion with $t_0, t_1 \neq 0$ are, in general, quite different from the localized fermion studied in Sec. IV A, the low-frequency anomalies are still governed by the same local coupling and remain qualitatively the same.

Let us first discuss here results for the case $t_1 \neq 0$, $t_0$=0, and $V$=0, which is of interest due to its relation with the analysis in Refs. 3 and 4. Off-diagonal terms in Eq. (4.3) vanish, so that we get two decoupled equations

$$\Sigma_{\pm}(\mathbf{k},\omega) = \frac{1}{(2\pi)^2} \int d^2q \, |\mathcal{U}_{\pm}(\mathbf{k},\mathbf{q})|^2 G_{\pm}(\mathbf{k}-\mathbf{q}, \omega - \omega_{\mathbf{q}}) \, . \tag{4.20}$$

We observe that Eq. (4.20) for $\Sigma_-$ is identical to the one used by Schmitt-Rink *et al.*,[3] and Kane *et al.*,[4] while $\sigma = +\frac{1}{2}$ excitations are not present in their approach. The only difference in $\Sigma_-$ is in the coupling constant. We get for the latter $2t_1$, what would correspond in a $t$-$J$ model[10] to $\frac{8}{3}t_{t-J}$, while Kane *et al.*[4] have $4t_{t-J}$. Equations (4.20) are regular at $q \to 0$, i.e., $\Sigma_-''(\mathbf{k},\omega > 0) \lesssim \omega^2$ as shown by Kane *et al.*[4]

In Fig. 7 we present some results for the QP spectra $A_{\pm}(\mathbf{k},\omega)$ as obtained by the numerical solution of Eqs. (4.20). The numerical method is identical to the one used in the case of the localized fermion. The only difference is in the $\mathbf{k}$ dependence of the SC equations, which puts more severe restrictions on the number of points in the $(\mathbf{k},\omega)$ space. We present in Fig. 7 results at the $\Gamma$ point, $\mathbf{k}$ =0, and at the $\Delta$ point, $\mathbf{k} = (\pi/2, \pi/2)$, for $A_+$ and $A_-$. We note that the $(-)$ band has a minimum at $\Delta$,[4] while for the $(+)$ band the minimum is at the $\Gamma$ point. It is interesting that for $V$=0 the lower appears to be the tripletlike $(+)$ band. We have to mention that

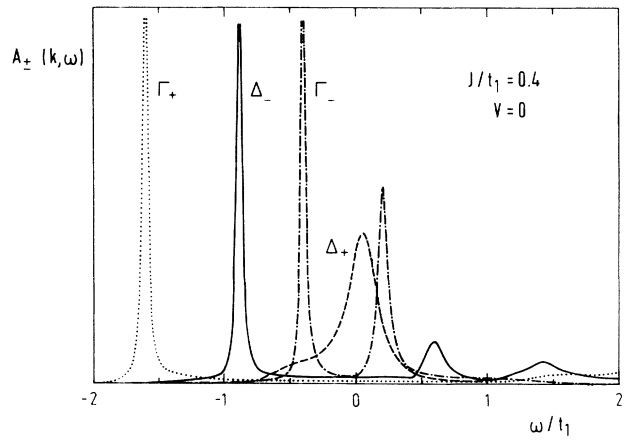


FIG. 7. Spectral functions $A_{\pm}(\mathbf{k},\omega)$, denoted with $\Gamma_{\pm}$ for $\mathbf{k} = (0,0)$ and $\Delta_{\pm}$ for $\mathbf{k} = (\pi/2, \pi/2)$ at $J/t_1$=0.4 and $V$=0.

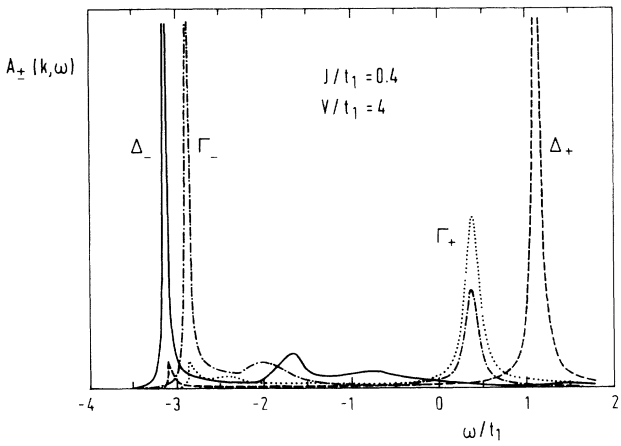


FIG. 8. The same as Fig. 7 for $J/t_1$=0.4 and $V/t_1$=4.

the *shape* of the band is very similar to the perturbative result $\Delta\varepsilon_{\mathbf{k}} = \Sigma'_{-}(\mathbf{k},0)$, by using in Eq. (4.20) $G_0(\mathbf{k},0)$ instead of $G(\mathbf{k},\omega)$.

If we switch on the diagonal part of the Kondo coupling $V_{\|}$, we shift $A_{\pm}(\mathbf{k},\omega)$ by an energy $\frac{1}{4}V_{\|}$ down and up, respectively. The shape of the spectra remain the same. So we obtain for larger $V_{\|}$, but still $V_{\perp} = 0$, the result of Kane *et al.*[4] as the lowest singletlike (−) band (neglecting already-mentioned differences in the width).

The transverse term $V_{\perp}$ couples additionally the (+) band with the (−) band, which causes the distortion and the narrowing of $A_+$ and $A_-$ spectra. We present in Fig. 8 spectra for $V/t_1$=4, again for Δ and Γ points. The lower band is centered around $\omega \sim -\frac{3}{4}V$, while the upper is at $\omega \sim +\frac{1}{4}V$. The distribution of the strength remains qualitatively analogous to the one in Fig. 3. In

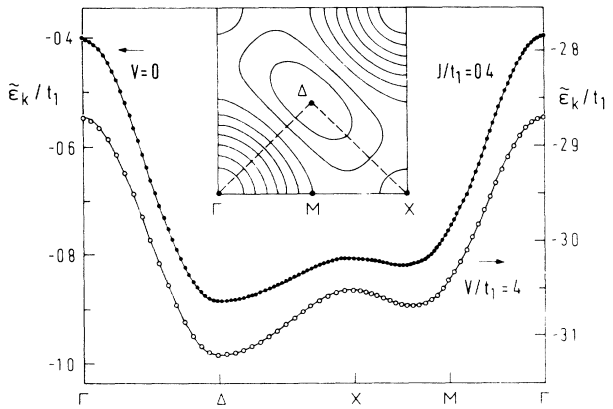


FIG. 9. $\sigma = -\frac{1}{2}$ energy bands $\tilde{\varepsilon}_{\mathbf{k}}$ in units of $t_1$. Left scale corresponds to $V$=0 case (•) and the right scale to the $V/t_1$=4 (o). Contour plot represents lines of constant $\tilde{\varepsilon}_{\mathbf{k}}$ for the $V/t_1$=4 case.

Fig. 9 we show the corresponding energy (−) bands $\tilde{\varepsilon}(\mathbf{k})$ as defined by the well-defined lower edge $\tilde{\varepsilon}_{\mathbf{k}} = \Sigma'(\mathbf{k},\tilde{\varepsilon}_{\mathbf{k}})$, throughout in the Brillouin zone. Note that the form of the bands at $V = 4t_1$ is not much changed with respect to the $V$=0 case, the main difference being the reduced width.

The tensor of the QP (coherent) effective mass enhancement $\boldsymbol{\mu}$ is defined by

$$\boldsymbol{\mu}^{-1} = \frac{1}{2t_1}\left(\frac{\partial^2\tilde{\varepsilon}_{\mathbf{k}}}{\partial\mathbf{k}\,\partial\mathbf{k}}\right), \tag{4.21}$$

calculated in the minimum, which is at the Δ point in the present case.

The eigenvalues of $\boldsymbol{\mu}$ are $\mu_{\|}$ along the direction Δ - Γ, and $\mu_{\perp}$ is along the direction Δ-$X$, where $X$ is the point $\mathbf{k} = (\pi,0)$. The anisotropy is defined as $\varepsilon = \mu_{\perp}/\mu_{\|}$. In Fig. 10 we show the smaller mass $\mu_{\|}$ and $\varepsilon$ as a function of $t_1/J$ for $V$=0 and $V = 4t_1$. The Kondo coupling of the fermion with magnons clearly increases the QP coherent mass. For $t_1/J \ll 1$ we obtain the perturbation result $\mu_{\|} \sim J/t_1$, while on the other side with $t_1/J \gg 1$ the SC approach yields $\mu_{\|} \sim t_1/J$.[4]

The results for $\mu_{\|}$ are in a good agreement with the numerical study[8] not only qualitatively but also quantitatively. In this respect our approach represents a quantitative improvement over the method by Kane *et al.* In such quantitative comparisons one has to take into account the relation between the hopping parameter in our model and in the $t$-$J$ model, $t_{t\text{-}J} = \frac{3}{4}t_1$.[10] Also the values for the anisotropy $\varepsilon \gg 1$ seem to correspond well to exact numerical results on small systems.

As already pointed out in Sec. III B the interaction

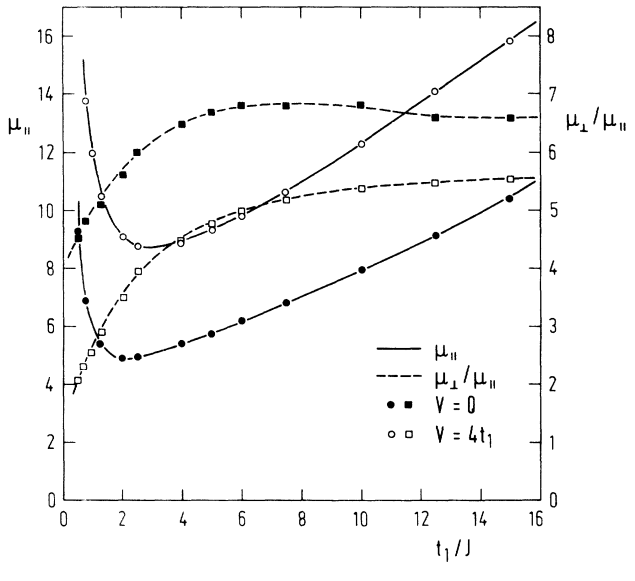


FIG. 10. Effective mass enhancement $\mu_{\|}$ is plotted for $V$ = 0 (solid circles) and for $V/t_1$=4 (open circles) vs $t_1/J$ (left scale). With dashed lines we denote the anisotropy $\mu_{\perp}/\mu_{\|}$ (right scale) for $V$=0 (solid squares) and $V/t_1$=4 (open squares).

$V$ with long-wavelength magnons acts equally on mobile and localized fermions. Hence the low-excitation spectra are governed by $V$ and not by $t_1$ terms in $\mathcal{H}_{\rm II}$. Numerical results for $\Sigma''$ in fact show low-frequency behavior as in the case of the localized particle ($t_1 \sim 0$).

## V. CONCLUSIONS

Let us first comment on the possible extension of our results to finite temperatures $T > 0$. The most interesting effect comes from the additional broadening of the QP peak due to the scattering on magnons excited at $T > 0$. For this case we just estimate $\Sigma''(T, \omega \sim 0)$, which can be related with QP inverse relaxation time $1/\tau$. Due to observed universal behavior, we perform a calculation for the localized case, $\mathcal{H}_{\rm II}$. Using the fourth-order perturbation expansion in $V_\perp$, as in Sec. III, and taking besides the emission processes in Figs. 1(b) and 1(c) also the absorption of magnons, we get

$$\Sigma''_{-}(T,0) \sim -\frac{V_\perp^4}{W^2}\mathrm{Im}\int d^2q \int d^2q' \frac{1}{c_0(q'-q)+i\eta}[(1+n_{\mathbf{q}})n_{\mathbf{q}'}u_{\mathbf{q}}{}^2u_{\mathbf{q}'}{}^2 - (1+n_{\mathbf{q}'})n_{\mathbf{q}}v_{\mathbf{q}}{}^2v_{\mathbf{q}'}{}^2] \sim \frac{V_\perp^4}{W^2 c_0}\int_0^{q_m}(1+n_q)n_q\, q\, dq\ , \tag{5.1}$$

where we use the identity $u_{\mathbf{q}}^4 - v_{\mathbf{q}}^4 = u_{\mathbf{q}}^2 + v_{\mathbf{q}}^2$ and $n_{\mathbf{q}} = (e^{\omega_{\mathbf{q}}/kT} - 1)^{-1}$, while leaving in Eq. (5.1) only the most important part corresponding to long-wavelength magnons $q \le q_m$. Here $W$ is equal to the level splitting $\frac{1}{2}V$, while in the analogous treatment of $\mathcal{H}_{\rm I}$ it would be $W \sim 8t_0$. At $T > 0$ the integral in Eq. (5.1) would logarithmically diverge, if we do not take into account that at the same time the AFM correlation length becomes finite, i.e., $\xi < \infty$, cutting off the integral at $q \sim \xi^{-1}$. Restricting ourselves to the low doping regime (few holes in an AFM), we can use for $\xi$ the $T$ dependence $\xi \sim e^{J/kT}$, obtained for Heisenberg antiferromagnet analytically[16] as well as experimentally in the undoped AFM.[17] Inserting this into Eq. (5.1) we obtain

$$\Sigma''(T,0) \sim \frac{V_\perp^4}{W^2 J}\left(\frac{kT}{J}\right)^2 \ln\xi(T) \sim \frac{V_\perp^4}{W^2 J^2}\, kT, \tag{5.2}$$

where higher-order terms in $T$ are left out. Such $T$ dependence would be in agreement with the generic behavior of the resistivity $\rho \propto T$ in copper oxides. However, our treatment of the QP at finite $T$ is too crude to allow any more definite conclusions.

Our results for $T$=0 as well as for $T > 0$ indicate that the strong coupling of the fermion to the long-wavelength AFM magnons, appearing mainly through the local Kondo-like interaction, leads to pronounced low-frequency anomalies. We obtain either $\Sigma''(\omega > 0) \propto \omega$ within the perturbation calculation, or $\Sigma''(\omega > 0) \propto \omega^{1/2}$ within the SC approach. In both cases the QP peak is not well defined in the strict sense even at $T$=0. These anomalies are not present if only hopping-induced interaction[3,4] is taken into account. Plausibly one can attribute these effects to the strong influence of a fermion (even a localized one), residing on one sublattice, on a state with a broken continuous symmetry. There are analogies with a two-level system, e.g., coupled with a piezoelectric-type coupling to acoustic phonons.[15] The nonanalytical self-energy and the vanishing $a_{\mathbf{k}} \to 0$ for the QP shows similarity with the orthogonality catastrophe encountered in the x-ray problem.[18] It should be noted that the most extensively studied $t$-$J$ model represents just the opposite limit $V \to \infty$ of the Kondo-lattice model discussed in this paper. Still we believe that the strong influence of the local coupling or constraint is more generic, giving to the holes in an AFM their quite intriguing properties.

## APPENDIX

In order to clarify the effect of the nonlinear term, Eq. (3.3), we perform the summation of all processes, containing at most a single magnon excitation in the intermediate state. This includes, e.g., diagrams in Figs. 1(a) and 1(d). This summation, including all the most divergent terms [as in Fig. 1(d)], can be formulated by an equivalent variational approach, where a trial wave function $|\psi_{\mathbf{k}-}\rangle$ takes into account all states of the fermion-magnon system that have at most a single excited magnon excitation:

$$|\psi_{\mathbf{k}-}\rangle = \left(a_{\mathbf{k}}c^\dagger_{\mathbf{k}-} + \bar{a}_{\mathbf{k}}c^\dagger_{\mathbf{k}+\mathbf{q}_0,-} + \sum_{\mathbf{q}}(b_{\mathbf{k}\mathbf{q}}c^\dagger_{\mathbf{k}-\mathbf{q},+} + \bar{b}_{\mathbf{k}\mathbf{q}}c^\dagger_{\mathbf{k}+\mathbf{q}_0-\mathbf{q},+})\alpha^+_{\mathbf{q}}\right)|0\rangle\ . \tag{A1}$$

Minimizing the expectation value of the QP energy

$$\lambda_{\mathbf{k}} = \frac{\langle\psi_{\mathbf{k}-}|\mathcal{H}_{\rm I}|\psi_{\mathbf{k}-}\rangle}{\langle\psi_{\mathbf{k}-}|\psi_{\mathbf{k}-}\rangle}\ , \tag{A2}$$

we get a set of coupled equations for $a_{\mathbf{k}}$, $\bar{a}_{\mathbf{k}}$, $b_{\mathbf{kq}}$, $\bar{b}_{\mathbf{kq}}$, and $\lambda_{\mathbf{k}}$

$$(\varepsilon_{\mathbf{k}} - \lambda_{\mathbf{k}})a_{\mathbf{k}} = \tfrac{1}{4}V_{\parallel}\bar{a}_{\mathbf{k}} - \tfrac{1}{4}V_{\perp}\sum_{\mathbf{q}}(\zeta_{\mathbf{q}}^{+}b_{\mathbf{kq}} + \zeta_{\mathbf{q}}^{-}\bar{b}_{\mathbf{kq}}) , \tag{A3}$$

$$(\varepsilon_{\mathbf{k}+\mathbf{q}_0} - \lambda_{\mathbf{k}})\bar{a}_{\mathbf{k}} = \tfrac{1}{4}V_{\parallel}a_{\mathbf{k}} - \tfrac{1}{4}V_{\perp}\sum_{\mathbf{q}}(\zeta_{\mathbf{q}}^{+}\bar{b}_{\mathbf{kq}} - \zeta_{\mathbf{q}}^{-}b_{\mathbf{kq}}) , \tag{A4}$$

$$(\varepsilon_{\mathbf{k}-\mathbf{q}} + \omega_{\mathbf{q}} - \lambda_{\mathbf{k}})b_{\mathbf{kq}} = -\tfrac{1}{4}V_{\perp}(\zeta_{\mathbf{q}}^{+}a_{\mathbf{k}} - \zeta_{\mathbf{q}}^{-}\bar{a}_{\mathbf{k}}) - \tfrac{1}{4}V_{\parallel}\bar{b}_{\mathbf{kq}} + \tfrac{1}{2}V_{\parallel}\sum_{\mathbf{q}'}f_{\mathbf{qq}'}\bar{b}_{\mathbf{kq}'} , \tag{A5}$$

$$(\varepsilon_{\mathbf{k}+\mathbf{q}_0-\mathbf{q}} + \omega_{\mathbf{q}} - \lambda_{\mathbf{k}})\bar{b}_{\mathbf{kq}} = -\tfrac{1}{4}V_{\perp}(\zeta_{\mathbf{q}}^{+}\bar{a}_{\mathbf{k}} + \zeta_{\mathbf{q}}^{-}a_{\mathbf{k}}) - \tfrac{1}{4}V_{\parallel}b_{\mathbf{kq}} + \tfrac{1}{2}V_{\parallel}\sum_{\mathbf{q}'}f_{\mathbf{qq}'}b_{\mathbf{kq}'} , \tag{A6}$$

where

$$\zeta_{\mathbf{q}}^{\pm} = u_{\mathbf{q}} \pm v_{\mathbf{q}} , \qquad f_{\mathbf{qq}'} = u_{\mathbf{q}}u_{\mathbf{q}'} + v_{\mathbf{q}}v_{\mathbf{q}'} , \tag{A7}$$

and

$$|a_{\mathbf{k}}|^2 + |\bar{a}_{\mathbf{k}}|^2 + \sum_{\mathbf{q}}(|b_{\mathbf{kq}}|^2 + |\bar{b}_{\mathbf{kq}}|^2) = 1 . \tag{A8}$$

The perturbational treatment of Eqs. (A3)–(A6), i.e., the expansion in $V_{\parallel}$, $V_{\perp}$, corresponds to first approximate (zeroth-order) $\lambda_{\mathbf{k}} \sim \varepsilon_{\mathbf{k}}$ and $a_{\mathbf{k}} = 1$ from Eq. (A3). This $\lambda_{\mathbf{k}} \sim \varepsilon_{\mathbf{k}}$ is used for the further iteration of the second set of Eqs. (A5) and (A6). Within the first order this gives $b_{\mathbf{kq}}$ and $\bar{b}_{\mathbf{kq}}$:

$$b_{\mathbf{kq}}^{(1)} = \tfrac{1}{4}V_{\perp}\frac{\zeta_{\mathbf{q}}^{+}}{\varepsilon_{\mathbf{k}} - \varepsilon_{\mathbf{k}-\mathbf{q}} - \omega_{\mathbf{q}}} , \quad \bar{b}_{\mathbf{kq}}^{(1)} = \tfrac{1}{4}V_{\perp}\frac{\zeta_{\mathbf{q}}^{-}}{\varepsilon_{\mathbf{k}} + \varepsilon_{\mathbf{k}-\mathbf{q}} - \omega_{\mathbf{q}}} . \tag{A9}$$

Using Eq. (A9) for $b_{\mathbf{kq}}$ to iterate Eqs. (A5) and (A6) yields among other terms also the second-order correction

$$\tilde{b}_{\mathbf{kq}}^{(2)} = -\frac{1}{2}\frac{V_{\parallel}}{\varepsilon_{\mathbf{k}} - \varepsilon_{\mathbf{k}-\mathbf{q}} - \omega_{\mathbf{q}}}\sum_{\mathbf{q}'}f_{\mathbf{qq}'}\bar{b}_{\mathbf{kq}'}^{(1)} \overset{q\to 0}{\longrightarrow} q^{-\frac{3}{2}} . \tag{A10}$$

This approximation leads directly to the logarithmic divergence of the corrections to $\lambda_{\mathbf{k}}$. The form of the divergence is exactly the same as that of the term corresponding to the diagram in Fig. 1(d). Not only the energy $\lambda_{\mathbf{k}}$ is divergent, but also the "number" of magnons involved in the QP,

$$N_{\mathrm{mag},\mathbf{k}} \sim \sum_{\mathbf{q}}(|b_{\mathbf{kq}}|^2 + |\bar{b}_{\mathbf{kq}}|^2) \to \infty , \tag{A11}$$

so the perturbational approach is not applicable to higher orders.

On the other hand, it is plausible that a proper (simultaneous) solution of Eqs. (A3)–(A6) does not contain such divergencies. Solving equations at fixed $V_{\parallel}$, $V\perp > 0$ we get as the main qualitative effect the shift of the unperturbed energies, i.e., $\lambda_{\mathbf{k}} \sim \varepsilon_{\mathbf{k}} - \varepsilon_b$, where $\varepsilon_b > 0$ and finite. Inserting this shift into Eqs. (A5) and (A6), we now also get no divergencies in $N_{\mathrm{mag}}$, etc. Nevertheless coefficients $b_{\mathbf{kq}}$ still show the asymptotic form

$$\tilde{b}_{\mathbf{kq}}^{(2)} = -\frac{1}{2}\frac{V_{\parallel}}{\lambda_{\mathbf{k}} - \varepsilon_{\mathbf{k}-\mathbf{q}} - \omega_{\mathbf{q}}}\sum_{\mathbf{q}'}f_{\mathbf{qq}'}\bar{b}_{\mathbf{kq}'}^{(1)} \longrightarrow q^{-\frac{1}{2}}$$

$$\text{as } q \to 0 , \tag{A12}$$

as in the perturbational form, Eq. (A9) or Eq. (3.1), within the lowest order in $V_{\perp}$. It is then plausible that perturbational result (3.1) is at least qualitatively correct, and, moreover, nonlinear terms do not change essentially the low-frequency behavior.

[1] W. F. Brinkman and T. M. Rice, Phys. Rev. B **2**, 1324 (1970).
[2] L. N. Bulaevskii, E. L. Nagaev, and D. I. Khomskii, Zh. Eksp. Teor. Fiz. **54**, 1562 (1968) [Sov. Phys. JETP **27**, 836 (1968)].
[3] S. Schmitt-Rink, C. M. Varma, and A. E. Ruckenstein, Phys. Rev. Lett. **60**, 2793 (1988).
[4] C. L. Kane, P. A. Lee, and N. Read, Phys. Rev. B **39**, 6880 (1989).
[5] Z. B. Su, Y. M. Li, W. Y. Lai, and L. Yu, Phys. Rev. Lett. **63**, 1318 (1989).
[6] J. Bonča, P. Prelovšek, and I. Sega, Phys. Rev. B **39**, 7074 (1989).
[7] E. Dagotto, A. Moreo, and T. Barnes, Phys. Rev. B **40**, 6721 (1989).
[8] I. Sega and P. Prelovšek, Phys. Rev. B **42**, 892 (1990).
[9] F. C. Zhang and T. M. Rice, Phys. Rev. B **37**, 3759 (1988).
[10] A. Ramšak and P. Prelovšek, Phys. Rev. B **40**, 2239 (1989).

[11] P. Prelovšek, Phys. Lett. A **126**, 287 (1988).
[12] J. Zaanen and A. M. Oleś, Phys. Rev. B **37**, 9423 (1988).
[13] For a review, see, e.g., T. M. Rice, Proceedings of the 9th General Conference of the Condensed Matter Division of EPS, Nice, 1989 [Phys. Scr. T **29**, 72 (1989)].
[14] N. Furukawa and M. Imada, J. Phys. Soc. Jpn. **59**, 771 (1990).
[15] C. B. Duke and G. D. Mahan, Phys. Rev. **139**, A1965 (1965); R. Pirc and B. G. Dick, Phys. Rev. B **9**, 2701 (1974).
[16] S. Chakravarty, B. I. Halperin, and D. R. Nelson, Phys. Rev. B **39**, 2344 (1989).
[17] K. Yamada, K. Kakurai, Y. Endoh, T. R. Thurston, M. A. Kastner, R. J. Birgeneau, G. Shirane, Y. Hidaka, and T. Murakami, Phys. Rev. B **40**, 4557 (1989).
[18] G. D. Mahan, *Many-Particle Physics* (Plenum, New York, 1990); P. W. Anderson (unpublished).